



# One-pot synthesis of aluminum oxide coating and aluminum doping on lithium manganese oxide nanoparticles for high performance energy storage system



Dong-Yo Shin <sup>a</sup>, Young-Geun Lee <sup>b</sup>, **Hyo-Jin Ahn** <sup>a, b, \*</sup>

<sup>a</sup> Program of Materials Science & Engineering, Convergence Institute of Biomedical Engineering and Biomaterials, Seoul National University of Science and Technology, Seoul 01811, South Korea

<sup>b</sup> Department of Materials Science and Engineering, Seoul National University of Science and Technology, Seoul 01811, South Korea

## ARTICLE INFO

### Article history:

Received 12 June 2017

Received in revised form

16 August 2017

Accepted 27 August 2017

Available online 30 August 2017

### Keywords:

Li-ion batteries

Lithium aluminum manganese oxide

Aluminum doping

Aluminum oxide coating

High-rate performance

## ABSTRACT

In the present study, in order to demonstrate the one-pot synthesis of aluminum oxide ( $\text{Al}_2\text{O}_3$ ) coating and aluminum doping, we synthesized aluminum oxide ( $\text{Al}_2\text{O}_3$ )-coated  $\text{LiAl}_x\text{Mn}_{2-x}\text{O}_4$  (LAMO) NPs using a sequential process of the as-spun nanofiber templates, chemical precipitation, and calcination as a cathode material in lithium ion batteries (LIBs). To find the optimum condition of  $\text{Al}_2\text{O}_3$  coating layer and Al doping, we performed the simple calcination methods at 300 °C using the  $\text{Al}(\text{OH})_2$ -coated LMO NPs. The resultant  $\text{Al}_2\text{O}_3$ -coated LAMO NPs exhibited the highest capacity of 111.1  $\text{mAh g}^{-1}$  with the capacity retention of 94.4% after 90 cycles at 1 C, excellent rate performance, and the highest high-rate capacity of 81.4  $\text{mAh g}^{-1}$  at 10 C as compared to bare LMO NPs without  $\text{Al}_2\text{O}_3$  coating and  $\text{Al}(\text{OH})_2$ -coated LMO NPs without calcination. The improved electrochemical performance can be defined by the co-effect of  $\text{Al}_2\text{O}_3$  coating and Al doping on bare LMO NPs. The former is related to cycle stability that increased due to the prevention of volume expansion and Mn dissolution as a physical buffer layer. The latter is related to high-rate performance improved due to the enhanced bonding energy of Al–O bond. Therefore, it can be concluded that  $\text{Al}_2\text{O}_3$ -coated LAMO NPs are promising candidate cathode materials for high-performance LIBs.

© 2017 Elsevier B.V. All rights reserved.

## 1. Introduction

Recently, energy storage devices, such as lithium ion batteries (LIBs), electrochemical capacitors, and fuel cells, have become the key technology to reduce the environmental pollution [1,2]. Among these energy storage devices, LIBs, with their advantages of high energy density ( $>150 \text{ Wh Kg}^{-1}$ ), excellent cycling stability ( $>1000$  cycles), low toxicity, and low memory effects, have been widely applied as high-performance power sources in mobile phones, electric vehicles (EVs), and energy storage system (ESS) [3,4]. In general, LIBs consist of four main components, namely, the anode, cathode, electrolyte, and separator. Among them, cathode materials are directly related to the electrochemical performance of LIBs [5–8]. To improve the electrochemical performance of LIBs, various

cathode materials, such as  $\text{LiMn}_2\text{O}_4$  (LMO),  $\text{LiCoO}_2$  (LCO),  $\text{LiNiO}_2$  (LNO), and  $\text{Li}(\text{Ni}_{0.33}\text{Co}_{0.33}\text{Mn}_{0.33})\text{O}_2$  (NCM), have been studied [9,10]. In particular, LMO has been extensively studied due to their advantages such as high theoretical capacity (148  $\text{mAh g}^{-1}$ ), excellent power density, low cost, widely voltage range, and eco-friendliness. Nevertheless, LMOs are still limited as cathode materials owing to their serious capacity fading and poor high-rate capacity [11]. To overcome this problem, various strategies, including morphology control (nanoparticles (NPs), nanorods, nanowires, and nanospheres), surface coating of metal oxide ( $\text{TiO}_2$ ,  $\text{ZrO}$ ,  $\text{ZnO}_2$ , and  $\text{CeO}_2$ ), and doping of metal (Sn, Ce, Ti, and Co) have been tried by many research groups [12–14]. These studies have demonstrated that the surface coating can enhance the cycling stability because it physically suppresses the destruction of LMO particles due to the prevention of volume expansion and Mn ion dissolution [15]. For example, Lai et al. fabricated the  $\text{TiO}_2$ -coated LMO NPs using the chemical precipitation method [16]. The  $\text{TiO}_2$ -coated LMO NPs showed the capacity of  $\sim 83.0 \text{ mAh g}^{-1}$  and the capacity retention of 90.0% after 90 cycles, because  $\text{TiO}_2$  coating used as a

\* Corresponding author. Program of Materials Science & Engineering, Convergence Institute of Biomedical Engineering and Biomaterials, Seoul National University of Science and Technology, Seoul 01811, South Korea.

E-mail address: [hjahn@seoultech.ac.kr](mailto:hjahn@seoultech.ac.kr) (H.-J. Ahn).

buffer layer prevented the volume expansion of LMO NPs. Furthermore, Zhao et al. synthesized the ZrO<sub>2</sub>-coated LMO NPs using the atomic layer deposition [17]. ZrO<sub>2</sub>-coated LMO NPs indicated the capacity of ~90.3 mAh g<sup>-1</sup> and the capacity retention of 71.1% after 100 cycles. The authors proposed that ZrO<sub>2</sub> coating prevented dissolution of Mn ions by a reduction of deleterious reaction at the LMO surface. In addition, in the case of doping effect, some researchers reported the fabrication of metal (Ga, Zn, and Gd)-doped LMO that causes the structural and chemical stability [18,19]. However, one-pot synthesis of Al<sub>2</sub>O<sub>3</sub> coating and Al doping on LMO NPs has not been reported yet. Therefore, aiming to demonstrate the co-effect of Al<sub>2</sub>O<sub>3</sub> coating and Al doping, in the present study, we synthesized aluminum oxide (Al<sub>2</sub>O<sub>3</sub>)-coated LiAl<sub>x</sub>Mn<sub>2-x</sub>O<sub>4</sub> (LAMO) NPs using a sequential process of the as-spun nanofiber templates, chemical precipitation, and calcination. In addition, we demonstrate the relationship between their electrochemical performance and the unique structure of Al<sub>2</sub>O<sub>3</sub>-coated LAMO NPs. The Al<sub>2</sub>O<sub>3</sub> coating layer on LMO surface has excellent physical/chemical stability, which prevents the Mn ion dissolution and the side reaction of electrolyte during the Li ion intercalation/deintercalation process.

## 2. Experimental

### 2.1. Synthesis of Al<sub>2</sub>O<sub>3</sub>-coated LiAl<sub>x</sub>Mn<sub>2-x</sub>O<sub>4</sub> (LAMO) nanoparticles (NPs)

Al<sub>2</sub>O<sub>3</sub>-coated LAMO NPs were fabricated using the as-spun nanofiber templates, chemical precipitation, and calcination. First, LMO NPs were synthesized by sol treatment using the as-spun nanofiber templates. To obtain the as-spun nanofiber templates, 10 wt% polyacrylonitrile (PAN, M<sub>w</sub> = 150,000 g mol<sup>-1</sup>, Aldrich) was dissolved in *N,N*-dimethylformamide (DMF, 99.8%, Aldrich) and stirred for 6 h. The prepared solution was put into the syringe equipped by a 23-gauge needle. Electrospinning was performed at the feeding rate of 0.03 ml h<sup>-1</sup> with the voltage of 13 kV. Aluminum foil collector was placed to 15 cm from the syringe needle. Thereafter, the as-spun nanofibers were added into the sol solution of 1 M lithium acetate dehydrate (CH<sub>3</sub>COOLi·2H<sub>2</sub>O, Aldrich) and 2 M manganese(II) acetate tetrahydrate ((CH<sub>3</sub>COO)<sub>2</sub>Mn·4H<sub>2</sub>O, Aldrich) in DI-water for 30 min. The sol treated as-spun nanofibers were dried at 80 °C and annealed at 700 °C for 10 h in air (referred to herein as bare LMO NPs). Second, to form the Al<sub>2</sub>O<sub>3</sub> coating layer on LMO NPs, chemical precipitation and calcination were performed. Aluminum isopropoxide (C<sub>9</sub>H<sub>21</sub>O<sub>3</sub>Al, Aldrich) and LMO NPs were solved in a mixed solution of ethanol and DI-water. Then, the prepared solution was heated at 90 °C for 30 min with stirring (referred to herein as Al(OH)<sub>2</sub>-coated LMO NPs). The calcination was performed at 300 °C in air for 3 h (referred to herein as Al<sub>2</sub>O<sub>3</sub>-coated LAMO NPs) to obtain the optimized Al doping and Al<sub>2</sub>O<sub>3</sub> coating. In this process, Al<sub>2</sub>O<sub>3</sub> coating and Al doping were simultaneously performed. Therefore, we obtained three different types of bare LMO NPs, Al(OH)<sub>2</sub>-coated LMO NPs, and Al<sub>2</sub>O<sub>3</sub>-coated LAMO NPs.

### 2.2. Characterization

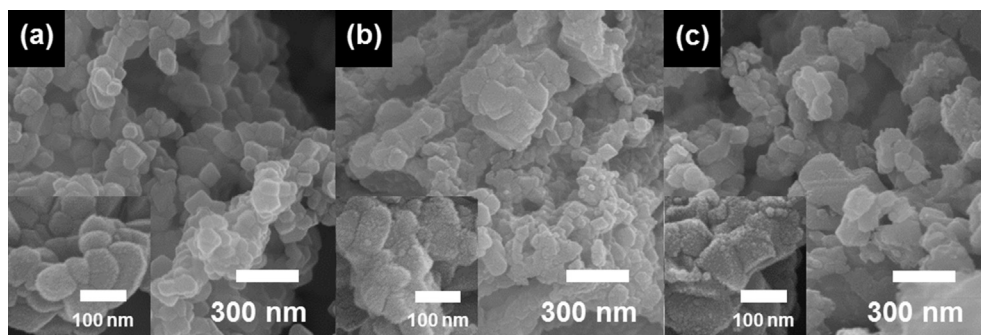
The structure and morphology properties of all samples were examined using field-emission scanning electron microscopy (FESEM; Hitachi S-4800) and transmission electron microscopy (TEM; JEOL, 2100F, KBSI Suncheon Center). TEM-EDS elemental mapping of Al<sub>2</sub>O<sub>3</sub>-coated LAMO NPs was carried out using a Phillips CM20T/STEM equipped with an energy-dispersive X-ray spectrometer (EDS). In addition, crystal structure and chemical bonding states were demonstrated using X-ray diffraction (XRD, Rigaku D/

MAX2500V) with Cu K $\alpha$  radiation in the angular range from 10° to 90° and X-ray photoelectron spectroscopy (XPS, ESCALAB250) with Al K $\alpha$  X-ray source under the base pressure of 267 nPa, respectively. Electrochemical measurements were performed using Li coin cells (CR2032, Hohsen Corporation) composed of Li metal foil (Honjo Chemical, 99.8%) as the anode, a porous polypropylene membrane (Celgard 2400) as the separator, the prepared samples as the cathode, and a 1.0 M LiPF<sub>6</sub> solution in a mixture of ethylene carbonate-dimethyl carbonate (1:1) as the electrolyte. To fabricate the cathode, slurries were prepared by the mixture of the sample (70 wt%) as the active material, poly(vinylidene difluoride) (20 wt%) as the binder, and ketjen black (10 wt%) as the conducting material (Alfa Aesar) in an *N*-methyl-2-pyrrolidinone solvent (NMP, Aldrich). The prepared slurry of all samples was coated on an Al foil substrate as the current collector. All electrodes were then dried at 100 °C for 12 h using the dry oven. The coin cells were fabricated in a high-purity argon-filled glove box (<5 ppm, H<sub>2</sub>O and O<sub>2</sub>). Electrochemical impedance spectroscopy (EIS) performance was investigated using a potentiostat/galvanostat (Eco chemie Autolab, PGSTAT302N) in the frequency range of 10<sup>5</sup> to 10<sup>-2</sup> Hz by applying the AC signal of 5 mV. The charge/discharge performance was measured using a WMPG 3000 battery cycler system (WonATech Corp., Korea) in the potential range of 3.0–4.5 V (versus Li/Li<sup>+</sup>) at 25 °C. The rate performance was investigated at current densities of 120 mA g<sup>-1</sup> (1 C), 360 mA g<sup>-1</sup> (3 C), 600 mA g<sup>-1</sup> (5 C), 840 mA g<sup>-1</sup> (7 C), 1200 mA g<sup>-1</sup> (10 C), and 120 mA g<sup>-1</sup> (1 C). Finally, electrochemical performance was measured after the aging test for 10 cycles.

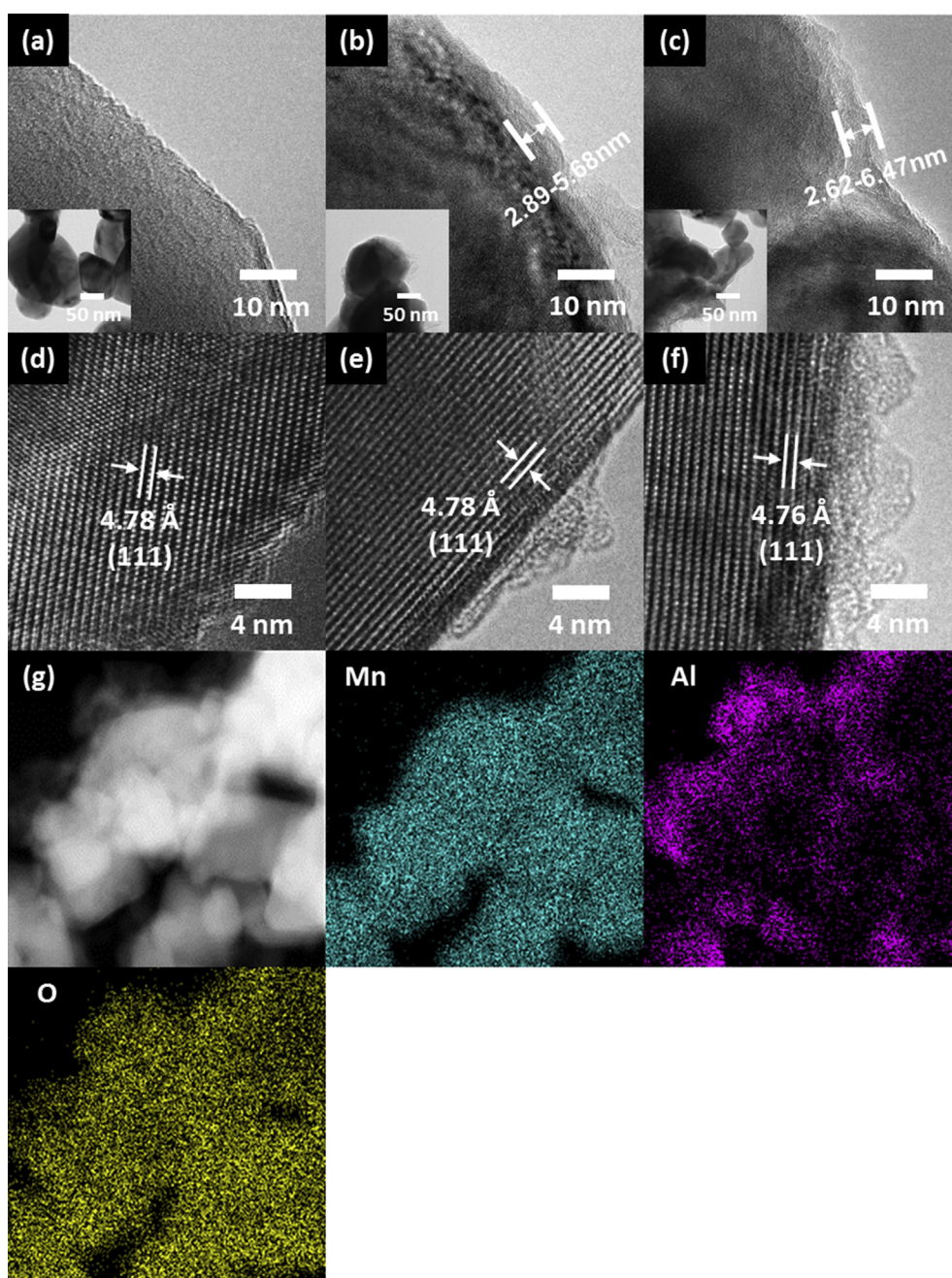
## 3. Results and discussion

Fig. 1 shows the FESEM images of bare LMO NPs, Al(OH)<sub>2</sub>-coated LMO NPs, and Al<sub>2</sub>O<sub>3</sub>-coated LAMO NPs. The diameters of bare LMO NPs, Al(OH)<sub>2</sub>-coated LMO NPs, and Al<sub>2</sub>O<sub>3</sub>-coated LAMO NPs are in the range from 113.6 to 138.1 nm, 118.2–141.3 nm, and 115.7–143.9 nm, respectively. The diameters of Al(OH)<sub>2</sub>-coated LMO NPs and Al<sub>2</sub>O<sub>3</sub>-coated LAMO NPs increased due to the formation of Al<sub>2</sub>O<sub>3</sub> coating layer. Bare LMO NPs were formed by the reaction of Li ion and Mn ion in as-spun nanofibers during the calcination at 700 °C. Furthermore, the Al(OH)<sub>2</sub>-coated LMO NPs and Al<sub>2</sub>O<sub>3</sub>-coated LAMO NPs shows the rough surface owing to the formation of the coating layer, as compared to bare LMO NPs (see the insets of Fig. 1a–c).

Fig. 2 presents low-resolution (a–c) and high-resolution (d–f) TEM images of bare LMO NPs, Al(OH)<sub>2</sub>-coated LMO NPs, Al<sub>2</sub>O<sub>3</sub>-coated LAMO NPs, and (e) TEM-EDS mapping image of Al<sub>2</sub>O<sub>3</sub>-coated LAMO NPs. Bare LMO NPs show a smooth surface without the Al<sub>2</sub>O<sub>3</sub> coating layer (see Fig. 2a). However, the surface of Al(OH)<sub>2</sub>-coated LMO NPs and Al<sub>2</sub>O<sub>3</sub>-coated LAMO NPs exhibits a dark contrast (core area) and a gray contrast (edge area), corresponding to LMO NPs and Al<sub>2</sub>O<sub>3</sub> coating layer, respectively. The coating layer thicknesses of Al(OH)<sub>2</sub>-coated LMO NPs and Al<sub>2</sub>O<sub>3</sub>-coated LAMO NPs are in the range from 2.89–5.68 nm to 2.62–5.47 nm, respectively. The Al<sub>2</sub>O<sub>3</sub> coating layer can increase the electrochemical stability due to the prevention of destruction of the LMO structure and Mn ion dissolution. For high-resolution images (see Fig. 2d–f), interlayer spacing of bare LMO NPs, Al(OH)<sub>2</sub>-coated LMO NPs, and Al<sub>2</sub>O<sub>3</sub>-coated LAMO NPs indicates ~4.78 Å, ~4.78 Å, and ~4.76 Å, corresponding to the (111) plane of the spinel LMO structure, respectively. In the case of bare LMO NPs and Al(OH)<sub>2</sub>-coated LMO NPs (see Fig. 2d–e), interlayer spacing shows the theoretical value of the (111) plane in the spinel LMO structure [20]. However, Al<sub>2</sub>O<sub>3</sub>-coated LAMO NPs show a lower interlayer spacing than bare LMO NPs and Al(OH)<sub>2</sub>-coated LMO NPs due to Al doping in LMO. In general, in the spinel LMO, it is well



**Fig. 1.** FE-SEM images of (a) bare LMO NPs, (b)  $\text{Al}(\text{OH})_2$ -coated LMO NPs, and (c)  $\text{Al}_2\text{O}_3$ -coated LMO NPs.



**Fig. 2.** TEM images of (a)–(c) low-resolution images, (d)–(f) high-resolution images of bare LMO NPs,  $\text{Al}(\text{OH})_2$ -coated LMO NPs, and  $\text{Al}_2\text{O}_3$ -coated LMO NPs, and (g) TEM-EDS mapping results of  $\text{Al}_2\text{O}_3$ -coated LMO NPs.

known that Li, Mn, and O ions locate the tetrahedral 8a sites, octahedral 16d sites, and 32e sites in the spinel structure [21]. For the doping process, the Al ions partially replace Mn(III) ions existing in octahedral 16d sites. Thus, interlayer spacing of spinel LMO decreased because the radius of Al(III) ion (0.053 nm) is smaller than the radius of Mn(III) ion (0.060 nm) and Mn(IV) ion (0.066 nm) [22]. To confirm the distributed composition of Mn, Al, and O elemental of Al<sub>2</sub>O<sub>3</sub>-coated LAMO NPs, TEM-EDS mapping was carried out (see Fig. 2g). The elemental mapping results indicate that the Al atoms are uniformly coated on the LAMO surface. In addition, O atoms are distributed overall owing to the existence of Al<sub>2</sub>O<sub>3</sub> and LMO.

To investigate the crystal structure of all samples, the XRD measurements were performed (see Fig. 3). The main characteristic diffraction peaks of bare LMO NPs are found at 18.6°, 36.1°, 43.9°, and 63.8°, corresponding to the (111), (311), (400), and (440) planes, respectively [23]. It is well-matched to spinel LiMn<sub>2</sub>O<sub>4</sub> with the space group of Fd-3m [JCPDS card No. 035-0782]. The (111) plan peak of Al(OH)<sub>2</sub>-coated LMO NPs is placed at the same position as bare LMO NPs owing to surface coating without surface doping of Al. However, diffraction peaks of Al<sub>2</sub>O<sub>3</sub>-coated LAMO NPs indicate a slight peak shift of 0.04° at a high angle, because the Al atoms with a small ion radius of 0.053 nm are doped at the LMO structure. Theoretically, the Al doping can improve the electrochemical performance owing to the strong bonding energy of Al–O bond (512 kJ mol<sup>-1</sup>) as compared to Mn–O bonding energy (402 kJ mol<sup>-1</sup>). In addition, for the Li ion insertion process, Li–Li repulsive force can be minimized, because it should be offset by the local distortion force of Al–O bond [22,24]. To demonstrate the doping effects according to the calcination temperature, we

calculated the Al(OH)<sub>2</sub>-coated LMO NPs at 400 °C and 500 °C. The diffraction peaks of these samples were shifted to higher angles when compared to Al<sub>2</sub>O<sub>3</sub>-coated LAMO NPs at 300 °C due to the excessive Al doping in LMO NPs, as shown in Fig. S1.

Fig. 4a–b shows the XPS spectra of the Mn 2p photoelectrons obtained from the bare LMO NPs and Al<sub>2</sub>O<sub>3</sub>-coated LAMO NPs. The Mn 2p spectral peak shows two different binding energies at ~642.4 eV (Mn 2p<sub>1/2</sub>) and ~654.1 eV (Mn 2p<sub>3/2</sub>). The Mn 2p<sub>3/2</sub> consisted of the Mn(III) (red area) and the Mn(IV) (blue area) states. Mn(III) and Mn(IV) exists in the 1:1 stoichiometric ratio in LMO (see Fig. 4a) [8]. In the case of Al<sub>2</sub>O<sub>3</sub>-coated LAMO NPs, Mn(III) peak is reduced with the formation of satellite peaks (yellow area) about Mn(IV) state by Al doping in LMO NPs (see Fig. 4b). The satellite peak of Al<sub>2</sub>O<sub>3</sub>-coated LAMO NPs is formed as follows. Occupied Mn ions at (001) surface of spinel LMO exist in the Mn(III) state due to the coordination of five O atoms, unlike in the case if the Mn ions bonded six O atoms in the spinel structure. However, in Al doping, the Mn(III) state at (001) surface is transformed to the Mn(IV) state due to the changed Fermi level of Mn ions by orbital of Mn 3d state [22,25,26]. This result means that Al is doped from exchanging the Mn(III) ion in the spinel LMO structure. For that reason, peak intensity of the Mn(III) state decreases with the formation of a satellite peak. Therefore, the formed Al<sub>2</sub>O<sub>3</sub> coating layer was demonstrated by the FESEM, TEM, and TEM-EDS results, and Al doping in LMO NPs was proved by the XRD and XPS data. We successfully fabricated the one-pot synthesis for the Al<sub>2</sub>O<sub>3</sub>-coated LAMO NPs.

To investigate the charge transfer kinetics, electrochemical impedance spectroscopy (EIS) test was performed before the galvanostatic charge-discharge test. Fig. 5a shows the Nyquist plot of

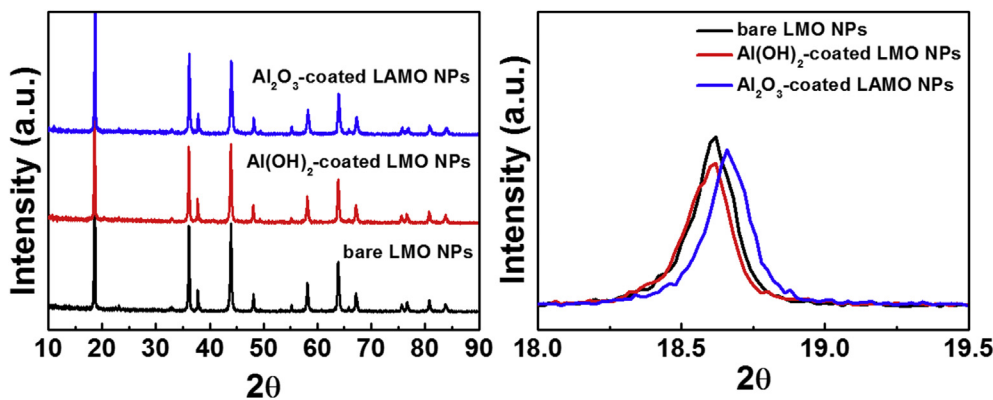


Fig. 3. XRD patterns of bare LMO NPs, Al(OH)<sub>2</sub>-coated LMO NPs, and Al<sub>2</sub>O<sub>3</sub>-coated LAMO NPs.

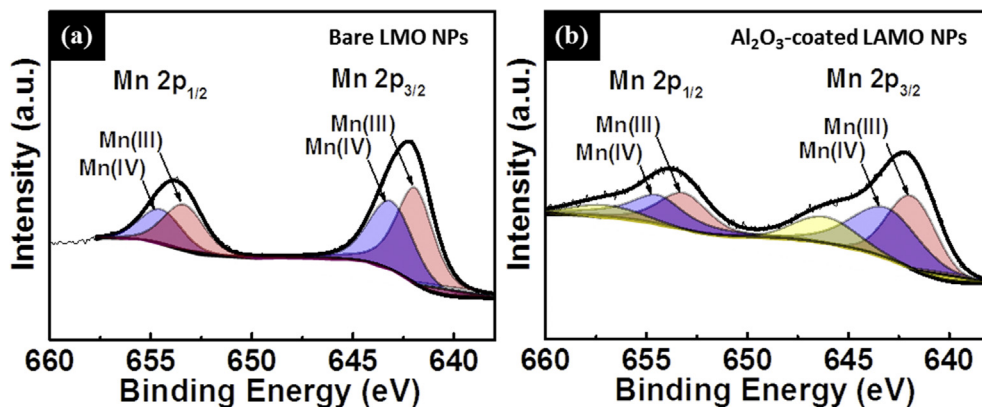


Fig. 4. XPS core-level spectra of Mn 2p obtained from (a) bare LMO NPs and (b) Al<sub>2</sub>O<sub>3</sub>-coated LAMO NPs.

bare LMO NPs, Al(OH)<sub>2</sub>-coated LMO NPs, and Al<sub>2</sub>O<sub>3</sub>-coated LMO NPs. The Nyquist plot is constructed by two regions. In the high-frequency region, the semicircle is related to the charge transfer rate ( $R_{ct}$ ) at the interface between the cathode and the electrolyte. In the low-frequency region, the straight line corresponds to the Li-ion diffusion into the cathode (referred to as Warburg impedance). In general, small semicircle diameters mean the low charge transfer resistance. Among them, the Al(OH)<sub>2</sub>-coated LMO NPs indicate the largest charge transfer resistance owing to Al(OH)<sub>2</sub> phase by the reaction between Li ion and OH ion [27,28]. However, Al<sub>2</sub>O<sub>3</sub>-coated LMO NPs showed a low charge transfer resistance owing to Al doping in LMO NPs.

Fig. 5b shows the charge-discharge curve of all electrodes at the current density of 1 C obtained after the aging test for 10 cycles. In the charge-discharge curve of all electrodes, two plateaus are observed at ~3.95 V and ~4.15 V, referring to the lithium ion intercalation and the deintercalation reaction in LMO. The electrochemical reaction can be represented by the Hunter equation [8] (see Eq. (1)).



The discharge capacity of bare LMO NPs, Al(OH)<sub>2</sub>-coated LMO NPs, and Al<sub>2</sub>O<sub>3</sub>-coated LMO NPs are observed as ~104.1 mAh g<sup>-1</sup>, ~89.9 mAh g<sup>-1</sup>, and ~121.8 mAh g<sup>-1</sup>, respectively. In this result, Al<sub>2</sub>O<sub>3</sub>-coated LMO NPs showed the highest reversible capacity due to Al<sub>2</sub>O<sub>3</sub> coating layer and optimum Al doping in LMO NPs.

Fig. 5c shows the cycling durability of all electrodes by galvanostatic charge-discharge tests up to 90 cycles after the aging test for 10 cycles. The electrodes of bare LMO NPs, Al(OH)<sub>2</sub>-coated LMO NPs, and Al<sub>2</sub>O<sub>3</sub>-coated LMO NPs exhibited the reversible capacity of 98.6 mAh g<sup>-1</sup> (capacity retention of 88.8%), 85.3 mAh g<sup>-1</sup> (capacity retention of 91.3%), and 111.1 mAh g<sup>-1</sup> (capacity retention of 94.4%) after 90 cycles, respectively. Bare LMO NPs exhibited a rapid

drop of specific capacity owing to the dissolution of Mn ions. As to Al(OH)<sub>2</sub>-coated LMO NPs, it showed a low specific capacity due to the presence of OH ions in Al(OH)<sub>2</sub> coating layer related to the interference of lithium insertion [27,28]. The Al<sub>2</sub>O<sub>3</sub>-coated LMO NP electrode indicated excellent cycling durability with a high specific capacity after 90 cycles, because it has favorable characteristics, such as the prevention of Mn ion dissolution and low repulsive force of Li ions [22,24,25]. However, for the calcination temperatures of 400 and 500 °C, Al<sub>2</sub>O<sub>3</sub>-coated LMO NPs showed relatively low specific capacity of 98.3 mAh g<sup>-1</sup> and 91.5 mAh g<sup>-1</sup> after 90 cycles due to the excessive Al doping in the LMO structure, leading to the destruction of spinel structure, as shown in Fig. S2.

Fig. 5d shows the rate performance of all electrodes at 1 C, 3 C, 5 C, 7 C, 10 C, and 1 C. The specific capacity of bare LMO NPs, Al(OH)<sub>2</sub>-coated LMO NPs, and Al<sub>2</sub>O<sub>3</sub>-coated LMO NPs at 10 C exhibited 8.4 mAh g<sup>-1</sup>, 37.5 mAh g<sup>-1</sup>, and 81.4 mAh g<sup>-1</sup>, respectively. In addition, when the current density returned to 1 C, their capacities were restored to 82.1%, 93.0%, and 98.5%, respectively. The increased electrochemical performance of Al<sub>2</sub>O<sub>3</sub>-coated LMO NPs can be the co-effect of Al<sub>2</sub>O<sub>3</sub> coating (Fig. 6a) and Al doping (Fig. 6b). First, the Al<sub>2</sub>O<sub>3</sub> coating layer prevents the dissolution of Mn ions due to the decreased disproportionation reaction at the LMO surface. Also, it acts as a buffer layer to prevent the destruction of bare LMO NPs owing to volume expansion [29]. Second, the Al doping in LMO NPs increases structural stability of spinel LMO. The doped Al atoms, which are located at octahedral 16d sites by replacing Mn<sup>3+</sup> ions, form a stronger Al–O bond (512 kJ mol<sup>-1</sup>) than Mn–O bond (402 kJ mol<sup>-1</sup>) [22]. In addition, a local distortion force is formed because the Al ion with a small ion radius of 0.053 nm replaces the Mn ion (radius of 0.060 nm). The local distortion force can assist the Li ion insertion into the LMO structure by a reduction of the Li–Li repulsive force [22,24,25]. Therefore, it can be concluded that Al<sub>2</sub>O<sub>3</sub>-coated LMO NPs are promising candidate cathode materials for high-performance LIBs.

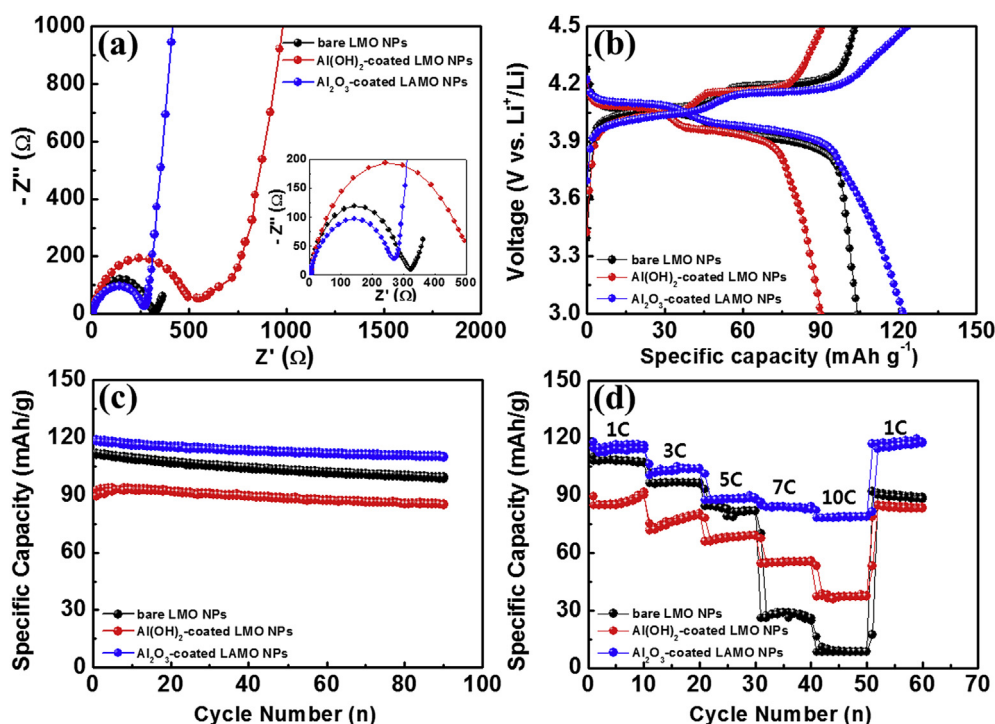


Fig. 5. (a) Nyquist plots in the frequency range of 100 kHz–100 mHz before the charge-discharge tests. (b) Galvanostatic charge-discharge curves of LIB cells fabricated with bare LMO NPs, Al(OH)<sub>2</sub>-coated LMO NPs, and Al<sub>2</sub>O<sub>3</sub>-coated LMO NPs. (c) The cycling number dependence of all samples up to 90<sup>th</sup> cycles at 1 C after aging test for 10 cycles. (d) The rate performance of all samples obtained from 1 C, 3 C, 5 C, 7 C, 10 C, and 1 C.

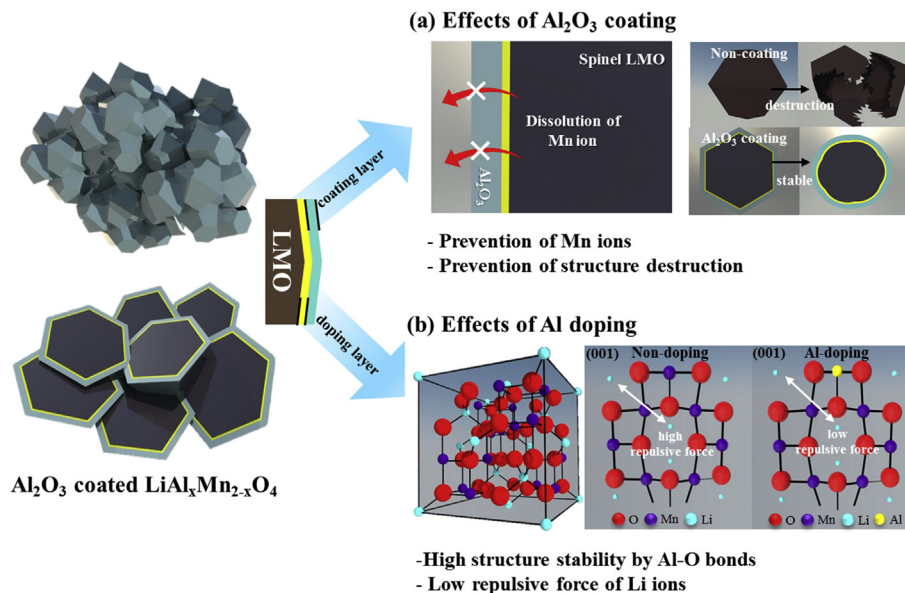


Fig. 6. Schematic illustration of co-effect by  $\text{Al}_2\text{O}_3$ -coated LAMO NPs.

#### 4. Conclusion

In this study,  $\text{Al}_2\text{O}_3$ -coated LAMO NPs were successfully synthesized by the as-spun nanofiber templates, chemical precipitation, and calcination. To simultaneously form  $\text{Al}_2\text{O}_3$  coating and Al doping on LMO, calcination at 300 °C was performed.  $\text{Al}_2\text{O}_3$ -coated LAMO NPs indicated the highest capacity of 111.1  $\text{mAh g}^{-1}$  (capacity retention of 94.4%) after 90 cycles at 1 C and excellent rate performance (81.4  $\text{mAh g}^{-1}$  at 10 C). The improved electrochemical performance can be explained by the co-effect of  $\text{Al}_2\text{O}_3$  coating and Al doping. First, increased cycle stability is attributed to  $\text{Al}_2\text{O}_3$  coating layer due to the prevention of Mn ion dissolution and volume expansion. Second, enhanced high-rate performance is related to Al doping owing to the formed Al–O bond and reduced Li–Li repulsive force. Therefore, we conclude that the co-effect of  $\text{Al}_2\text{O}_3$  coating and Al doping on LMO NPs using the one-pot synthesis has a great potential for high-performance LIBs.

#### Acknowledgement

This work was supported by the Industrial Fundamental Technology Development Program (10052745, Development of nano-sized (100 nm) manganese ceramic material for high voltage pseudo-capacitor) funded by the Ministry of Trade, Industry and Energy (MOTIE) of Korea.

#### Appendix A. Supplementary data

Supplementary data related to this article can be found at <http://dx.doi.org/10.1016/j.jallcom.2017.08.252>.

#### References

- [1] A.R. Armstrong, P.G. Bruce, *Nature* 381 (1996) 499–500.
- [2] G.-H. An, E.-H. Lee, H.-J. Ahn, *Phys. Chem. Chem. Phys.* 18 (2016) 14859–14866.

- [3] G.-H. An, J.I. Sohn, H.-J. Ahn, *J. Mater. Chem. A* 4 (2016) 2049–2054.
- [4] D. Ruan, Y. Huang, L. Li, J. Yuan, Z. Qiao, *J. Alloys Compd.* 695 (2017) 1685–1690.
- [5] B. Zhou, H. Shi, R. Cao, X. Zhang, Z. Jiang, *Phys. Chem. Chem. Phys.* 16 (2014) 18578–18585.
- [6] D.-Y. Sin, B.-R. Koo, H.-J. Ahn, *J. Alloys Compd.* 696 (2017) 290–294.
- [7] W. Li, A. Dolocan, P. Oh, H. Celio, S. Park, J. Cho, A. Manthiram, *Nat. Commun.* 8 (2017) 1–10.
- [8] H. Meng, L. Li, J. Liu, X. Han, W. Zhang, X. Liu, Q. Xu, *J. Alloys Compd.* 690 (2017) 256–266.
- [9] M.-J. Lee, S. Lee, P. Oh, Y. Kim, J. Cho, *Nano Lett.* 14 (2014) 993–999.
- [10] S. Tao, F. Kong, C. Wu, X. Su, T. Xiang, S. Chen, H. Hou, L. Zhang, Y. Fang, Z. Wang, W. Chu, B. Qian, L. Song, *J. Alloys Compd.* 705 (2017) 413–419.
- [11] Q. Zhu, S. Zheng, X. Lu, Y. Wan, Q. Chen, J. Yang, L.-Z. Zhang, Z. Lu, *J. Alloys Compd.* 654 (2016) 384–391.
- [12] H.-W. Ha, N.J. Yun, K. Kim, *Electrochim. Acta* 52 (2007) 3236–3241.
- [13] K. Raju, F.P. Nkosi, E. Viswanathan, M.K. Mathe, K. Damodaran, K.I. Ozoemena, *Phys. Chem. Chem. Phys.* 18 (2016) 13074–13083.
- [14] X. He, J. Li, Y. Cai, Y. Wang, J. Ying, C. Jiang, C. Wan, *J. Power Sources* 150 (2005) 216–222.
- [15] S.-C. Park, Y.-M. Kim, Y.-M. Kang, K.-T. Kim, P.S. Lee, J.-Y. Lee, *J. Power Sources* 103 (2001) 86–92.
- [16] C. Lai, W. Ye, H. Liu, W. Wang, *Ionics* 15 (2009) 389–392.
- [17] J. Zhao, Y. Wang, *Nano Energy* 2 (2013) 882–889.
- [18] H. Goktepe, H. Sahar, S. Patat, A. Ulgen, *Ionics* 15 (2009) 233–239.
- [19] S.C. Han, S.P. Singh, Y.-H. Hwang, E.G. Bae, B.K. Park, K.-S. Sohn, M. Pyo, *J. Electrochem. Soc.* 159 (2012) A1867–A1873.
- [20] Y.-L. Ding, J. Xie, G.-S. Cao, T.-J. Zhu, H.-M. Yu, X.-B. Zhao, *Adv. Funct. Mater.* 21 (2011) 348–355.
- [21] Q. Liu, S. Wang, H. Tan, Z. Yang, J. Zeng, *Energies* 6 (2013) 1718–1730.
- [22] C.Y. Ouyang, X.M. Zeng, Z. Slijivancanin, A. Baldereschi, *J. Phys. Chem. C* 114 (2010) 4756–4759.
- [23] Y.-K. Sun, M.-J. Lee, C.S. Yoon, J. Hassoun, K. Amine, B. Scrosati, *Adv. Mater.* 24 (2012) 1192–1196.
- [24] J.L. Wang, Z.H. Li, J. Yang, J.J. Tang, J.J. Yu, W.B. Nie, G.T. Lei, Q.Z. Xiao, *Electrochim. Acta* 75 (2012) 115–122.
- [25] Y.-S. Lee, N. Kumada, M. Yoshio, *J. Power Sources* 150 (2001) 376–384.
- [26] D. Liu, X. Liu, Z. He, *J. Alloys Compd.* 436 (2007) 387–391.
- [27] J. Xiang, C. Chang, M. Li, S. Wu, L. Yuan, J. Sun, *Cryst. Growth Des.* 8 (2008) 280–282.
- [28] P. Lian, X. Zhu, S. Liang, Z. Li, W. Yang, H. Wang, *Electrochim. Acta* 55 (2010) 3909–3914.
- [29] K.A. Walz, C.S. Johnson, J. Genthe, L.C. Stoiber, W.A. Zeltner, M.A. Anderson, M.M. Thackeray, *J. Power Sources* 195 (2010) 4943–4951.